Graduate School of Neural & Behavioural Sciences

Faculty of Science

Faculty of Medicine

Eberhard Karls Universität Tübingen

Detection of linear ego-acceleration from optic flow in stereoscopy

Thesis

submitted in partial fulfilment of the requirements of the degree

Master of Science

Till Becker

till.becker@uni-tuebingen.de

March 27, 2013

First Reader:

Prof. Dr. Hanspeter Mallot,

Cognitive Neuroscience,

Department of Biology,

Eberhard Karls Universität Tübingen

Germany

Second Reviewer:

Prof. Dr. Frank Schaeffel,

Centre for Ophthalmology, Institute of Ophthalmic Research,

Section of Neurobiology of the Eye

Eberhard Karls Universität Tübingen

Germany

Supervisor:

Dr. Gregor Hardiess,

Cognitive Neuroscience,

Department of Biology,

Eberhard Karls Universität Tübingen

Germany

The aim of this study was to investigate if subjects can use information from binocular disparity and optic flow to judge ego-acceleration. For this purpose, a stereoscopic setup was extended and validated for accuracy of disparities. Subjects viewed random-dot stereograms of a narrowing, a straight, and a widening tunnel. Psychometric functions of the perception of varying ego-accelerations were fitted. The results showed that subjects confuse actual ego-acceleration and scene geometry. Previous work in a similar two-dimensional setup suggested that the matched-filter approach for the estimation described the results well. This approach does not take depth information into account. An alternative approach, the acceleration rate that depends on retinal flow fields, had to be rejected. In the present study former results were compensated to some degree. However, even though a depth cue from binocular disparity was offered, subjects could not fully disentagle actual ego-acceleration and scene geometry.

Affirmation

I hereby confirm that my thesis is the result of my own work. All sources and/or materials applied are listed and specified in the thesis.

Eidesstattliche Erklärung

Hiermit erkläre ich, dass ich diese Arbeit selbst verfasst und keine anderen als die angegebenen Quellen und Hilfsmittel benutzt habe.

Tübingen, March 27, 2013

Acknowledgment

I want to thank Prof. Dr. Hanspeter Mallot for accepting me to work on this subject and for being a great and patient teacher. I also appreciate that Prof. Dr. Schaeffel took the role of the second reviewer.

Special thanks to my supervisor Dr. Gregor Hardiess for countless hours of discussions about work and not only.

I found great support in Dr. Hans-Jürgen Dahmen while working on the stereoscopic setup. I am also deeply grateful that he shared some of his great wisdom about life in general with me.

Fabian Recktenwald helped me to get to the next step of my programming skills, gave considerate advices and took a big part in rewriting the software.

Freya Festl, Matthias Hannig, and Marc Halfmann helped me jump-start on this journey. This work was based to a large extent on their previous achievements.

Contents

1. Introduction

1.1. Estimation of Ego-Motion

Most animals including insects and vertebrates need a precise mechanism for estimation and control of ego-motion as they navigate in three-dimensional space. Navigation and also object avoidance rely largely on the visual information. It has been shown that optic flow was used in translational heading during locomotion (Warren et al. [1988]). However, when moving in a given direction, the optic flow field cannot differentiate between a far object that moves fast and a slow object close by. Hence, translational velocity cannot be recovered from optic flow because projected translational flow depends only on the ratio of ego-motion and the distance of a feature point. As a result, optic flow seems not to be sufficient to calculate ego-velocity and in consequence ego-acceleration.

In object avoidance tasks, both ego-motion and the geometry of the three-dimensional space have to be considered. The distance to an approaching target and translational speed are taken into account for the estimation of time-to-collision (TTC) and time-to-passage (Kaiser and Hecht [1995]). Given a point in space, a frontoparallel plain can be estimated. This virtual plain can be used to calculate the TTC. After passing certain amount of time, the estimate of the TTC can be updated and compared to previous estimates. If now the amount of the TTC increased, an acceleration has to be occurred (Capelli et al. [2010]). Kaiser and Hecht [1995] proposed evidence for at least some degree of both acceleration and deceleration. These results however seem contradictory to the fact that both TTP and TTC depend largely on optic flow.

1.2. Ego-Acceleration from Optic Flow

Two approaches concerning the estimation of ego-acceleration in pure translational movement in the direction of its optical axis can be formulated. Both were described in more detail in Festl et al. [2012].

First, a feature-based acceleration rate approach can be described as in Kaiser and Hecht [1995]. It has been shown that the acceleration rate can be defined as the ratio of the acceleration and velocity which is then independent of scene geometry (figure 1.1a). In pure translational heading in z-direction, optic flow velocity is defined as $\dot{z}$ (first order derivative), and acceleration as $\ddot{z}$ (second order derivative). A feature point p is projected onto the image plane of a moving camera and p is tracked over time. The acceleration rate ρ defined as the ratio of acceleration and velocity $\ddot{z}/\dot{z}$ and can be calculated from the point p tracked over time:

$$\rho := \frac{\ddot{z}}{\dot{z}} = \frac{\ddot{p}}{\dot{p}} - 2\,\frac{\dot{p}}{p}. \tag{1.1}$$

Second, the matched-filter approach has been formulated by Franz et al. [2004], see figure 1.1b. This approach assumes that retinal motion vectors should be longer the faster the observer is moving when depth does not change over time. An expected flow field is compared with a sensed flow field of an image point projected to the retina, see figure 1.1b. Neural correlates have been found both in bees and primates that offer reference fields for known ego-motion patterns (Franz et al. [2004], Yu et al. [2010]). To formulate this approach, a few variables have to be defined. The expected flow field $u(p)$ is defined by the vector of the retinal coordinates p and the expected flow vector u. In a simple environment (as a tubular tunnel) the expected flow vector can then be defined as the radial pattern of unit vectors, $u(p) = p/\parallel p \parallel$. An estimate of ego-velocity, v^*, can then be determined by projecting the actual retinal motions $\dot{p}$ onto the locally expected vector $u = p/\parallel p \parallel$ and summing the results over the visual field. Finally, A is the area of the visual field and the integral is taken over the entire visual field:

$$v^* = \frac{v_0}{A} \int \frac{(p \cdot \dot{p})}{\parallel p \parallel}\, dp. \tag{1.2}$$

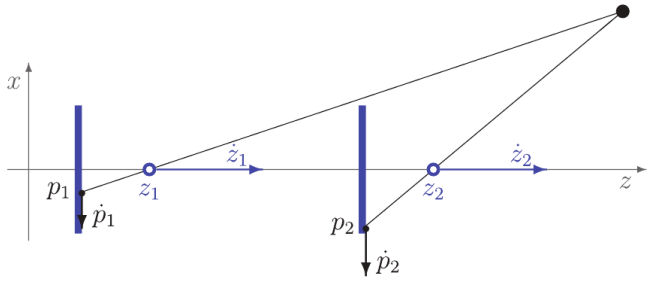

(a) Feature-based acceleration rate approach

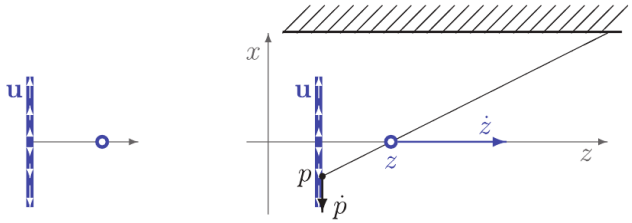

(b) Matched filter approach

Figure 1.1.: Two approaches to ego-acceleration estimation from optic flow. Camera frames are symbolized by an image plane (blue bars) and a nodal point (open blue circles) with position labels z, z_1, or z_2. The observer is moving along the z-axis at a speed $\dot{z}$. Image points are marked by the letter p, image motions by $\dot{p}$. *Top*: Two frames in the feature-based acceleration rate approach. A feature is tracked over time to measure its retinal acceleration. From this, ego-acceleration is calculated using acceleration rate. *Bottom*: Matched-filter approach in an environment with constant depth distribution. Left: For a particular motion pattern and environment, an expected vector-field $u(p)$ exists, which is symbolized in the figure by the white arrows appearing within the image plane. Right: Ego-motion and ego-acceleration can then be estimated from a comparison of the expected flow field with the actually sensed field. Source Festl et al. [2012].

Festl et al. [2012] showed that subjects completely confuse ego-acceleration and three-dimensional structure of the scene in a monocular viewing task. Hence, observers performance could be explained following the second approach (matched-filter approach) where scene depth is not taken into account. If however depth information could have been processed, the first approach (acceleration rate approach) should have been enable to disentangle effects of actual ego-acceleration and environment shape.

1.3. Cue Integration of Ego-Motion and Stereopsis

A large body of research covers the mechanisms about how to extract depth information of the environment from vision. Several features can be processed during ego-motion to estimate the three-dimensional shape of the world, including structure from motion, motion parallax, and binocular disparity. It is thought that different cues are first processed separately and the results of the different estimates is then combined.

Rogers and Collett [1989] and Tittle and Braunstein [1993] showed how cues from motion parallax and structure from motion together with binocular disparity can be integrated. Both studies showed that the performance of observers decreased when one of the two cues was either completely absent or when the information that could be extracted from that cue was reduced. When the information of two different cue is combined, the brain can derive more accurate and robust estimates of the three-dimensional geometry of the world.

Several types of useful integration between cues can be thought of as listed in Bulthoff and Mallot [1988]. Two of these types seem applicable in this context. In the case of accumulation, information of different cues is integrated in different ways, such as probablity summation and linear summation. Cooperation denotes a nonlinear intergration of different cues. Additionally, a wide spread modern approach is the Bayesian model of sensory cue integration. This is a statistical approach that combines sensory information with prior knowledge about the world.

1.4. Aim of this study

In a recent work by Festl et al. [2012] it was studied if subjects were able to estimate ego-acceleration from optic flow. For this purpose, psychometric functions were fitted of the perception of acceleration when observing simulated flights through cylindrical and conic (narrowing and widening) tunnels. The stimuli provided random dots fields to offer information from optic flow. Festl et al. [2012] found that subjects did not disentangle effects of actual ego-acceleration and environment shape. This finding

supported the matched-filter approach to the estimation of ego-acceleration. Observers ignored acceleration rate and confused a narrowing tunnel shape as an acceleration and a widening tunnel shape as a deceleration. Variations of dot lifetime affected the results only marginally.

The present study aims to further investigate the above results by offering a depth cue from binocular disparity. For this purpose, subjects viewed similar random dot stereogram stimuli as in the Festl et al. [2012] study in a stereoscopic setup. Both, the same tunnel shapes (narrowing, straight, and widening) as well as the same acceleration conditions ranging from $-5.5\ {}^{m}/_{s^2}$ deceleration to $5.5\ {}^{m}/_{s^2}$ acceleration were presented. A long dot lifetime of 1 *sec* was chosen. Psychometric functions were fitted and analyzed to determine the point of subjective equality (PSE). Two series of experiments were conducted. In the first experiment subjects viewed the stimuli binocularly, in the second experiment subject viewed the same stimuli in a monocular setting. The second experiment aimed to replicate the findings in Festl et al. [2012] and to rule out effects of the binocular viewing and the new experimental setup.

If humans can use the depth information from binocular disparity an estimation of the acceleration rate, the confusion of ego-acceleration and environment shape should be reduced or even fully compensated. Hence, the thresholds at which subjects perceive a certain amount of acceleration as acceleration or deceleration would be independent of the three-dimensional structure of the scene. As a result, psychometric functions of for conic tunnels should fall together with psychometric functions for tubular tunnels. However, if depth information is ignored or cue integration from binocular disparity and optic flow fails, the matched-filter approach would be expected to cause shifted psychometric functions.

2. Methods

2.1. Stereoscope Setup

This section describes in detail the stereoscope setup, including both the hardware and its modifications and additions to previous work, as well as the software that was used to conduct the experiment. Further, some test procedures that has been carried out to assure the correct operation of the setup will be explained.

2.1.1. Stereoscope Hardware

Wheatstone [1852] firstly described the original idea of a stereoscope about one and a half centuries ago by using two mirrors to project two different images on each eye. This setup has been largely simplified according to Kollin and Hollander [2007] by letting the observer watch one image straight and using only one mirror to redirect the gaze on a second image, see figure 2.1. This new setup reduces largely the degrees of freedom of the mechanical parts of the system. In such a setup, position and orientation of the monitors and the mirror have to be well adjusted to provide a perfect match of the two images for the observer.

As described in Hannig [2012], a custom built stereoscope was used in this study. The stereoscope was rebuilt to fit on a smaller arrangement by placing the left monitor to a smaller angle than 90°. In doing so, the setup could be fitted on a single table offering also a better seating position for the experiment's participant. The operating personal computer was the same as in the Hannig [2012] setup, see the full setup in figure 2.1 .

The setup included one surface mirror right in front of the face of the observer and

two monitors of 27″ diagonal screen size at a distance of approximately 80 cm to the observer. The horizontal field of view thus spans approximately 41.11° and the vertical field of view about 23.65°. With a resolution of 2560×1440 pixel, a single pixel was 0.232 mm in side length, i.e. an viewing angle of 0.016°. An eye separation of 6.5 cm was used for all subjects.

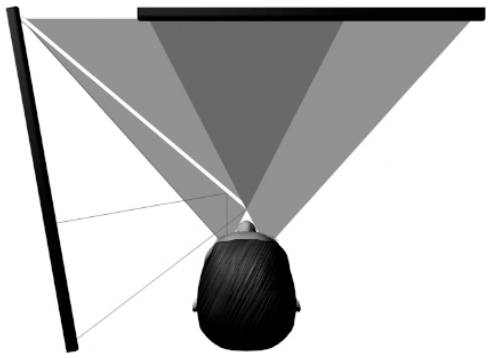

Figure 2.1.: Stereoscopic One-Mirror-Setup as in Kollin and Hollander [2007]. The sight of the right eye is directly to the screen (black line) whereas a mirror (white line) is used to look to the left screen with the other eye.

2.1.1.1. Calibration

To achieve an optimal visual experience, the images of both monitors have come to a match by adjusting both the orientation of monitors and the mirror. Such an adjustment must handle a large number of degrees of freedom. The monitors had a fixed height, but still offer all of yaw, pitch and roll originating from the self constructed stands. Also the mirror provides all degrees of freedom. To better handle the degrees of freedom of the mirror, a new connecting piece between the lower and the upper stand was built for smoother turning while calibrating.

Calibration itself worked best by first positioning the monitor for the right eye in straight frontal position to the observer. The monitor for the left eye and the mirror to some meaningful orientation while the mirror should have an angle such that the observers face is not reflected. To achieve best vertical and horizontal positions of the elements, it was most convenient to align these by pure eye-sight the edges of the elements with others

provided in the lab (e.g. pillars of the building). Next, monitors and mirror were brought to vernier adjustment by setting the edges of the two monitors to complete match while looking through the mirror.

Besides such a calibration procedure, it should that be noted that the stereoscopic perception was very robust, i.e. the three-dimensional perception could also easily be established even with a non-optimal calibration.

2.1.1.2. Building a Viewing Chamber

The experiment was conducted in a completely against daylight darkened environment. It had to be taken into account that the LCD panels of the monitors themselves produce a lot of light, even when displaying a black image. To enhance the immersive effect and the contrast of the images displayed on the monitors for each eye respectively, a viewing chamber was built, that separates the image of each monitor completely for each eye creating two separated viewing tunnels. To close the viewing tunnels from above, the whole setup was covered by a 130 cm $\times$ 100 cm light weight wooden panel that rests on metal stands. In order to not affect the calibration, the panel was placed some millimeters above the monitors, such that the panel does not rest on the monitors. The bottoms of the viewing tunnels consisted of two wooden panels fitting the geometry of the setup. These two bottom panels were screwed on a custom built metal plate that was mounted on metal stands. The mount can be tilted about the horizontal axes. All inside surfaces of the wooden panels facing the inside of the viewing tunnels were painted with matte black dispersion paint to reduce reflection. The walls of the viewing tunnel consist of black cotton that was pinned on a wooden lath attached to the covering panel.

The viewing chamber was built to suffice a list of requirements. It should be low-priced, light weight, and easy to setup and remove. Further it was constructed to be as modular as possible, i.e. all parts can be used (at least to some degree) for a different kind of a stereoscopic device.

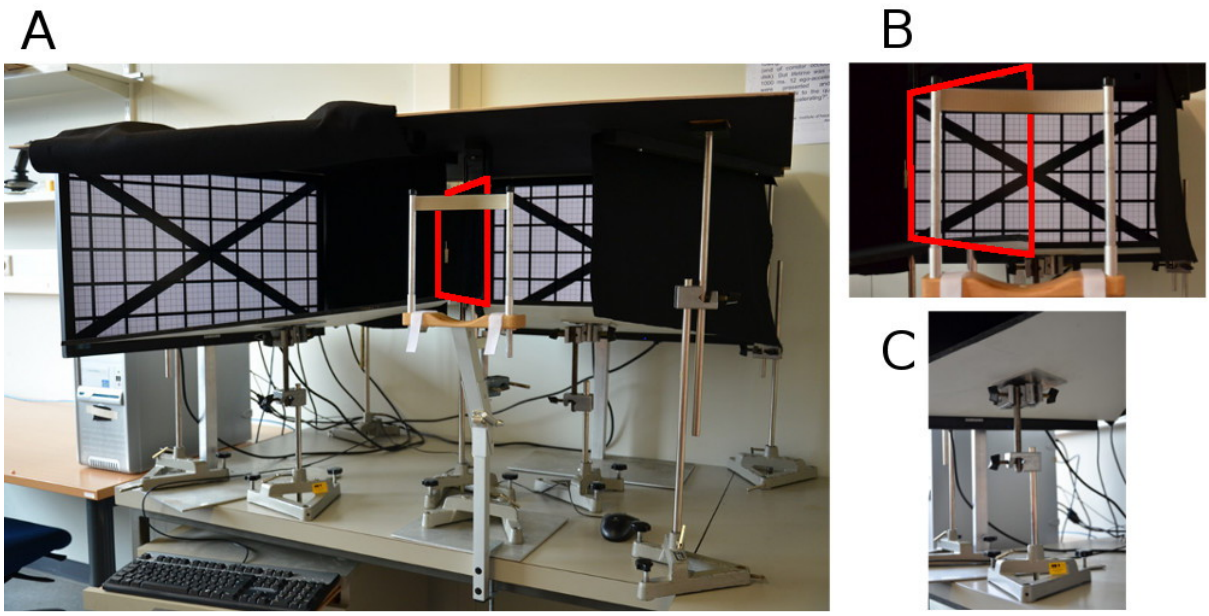

Figure 2.2.: **A**: Shows the setup from the front with one cotton wall opened up, in the middle the chin rest with the mirror right behind, on the left the left monitor, the right monitor on the right inside the chamber. The mirror is marked by a red box. **B**: The view from the observer position. When sitting in place the left eye only sees the mirrored image of the left monitor, the right eye looks past the mirror on the right screen. The mirror is marked by a red box. **C**: The mount for the bottom of the viewing tunnel.

2.1.1.3. Validating the Stereoscope

When generating an image of a scene on a screen, i.e. from the scene world coordinate system to camera coordinate system, the used software library had to perform a number of transformations on the coordinates of the objects. To validate the stereoscopic setup (hardware and software), a test has been conducted ensuring that the disparities are rendered and displayed in a correct manner. Therefore, a scene was created consisting of three colored poles (blue, red and green) in distances of 1, 2 and 3 meters to the origin, see figure 2.4A.

The resulting disparities were measured as the gaps between the poles displayed using a ruler. Disparities were calculated as in figure 2.4C. Defining object distances from the origin as D_1, D_2, and the distance difference $\Delta D = D_2 - D_1$, D_1 was calculated with the

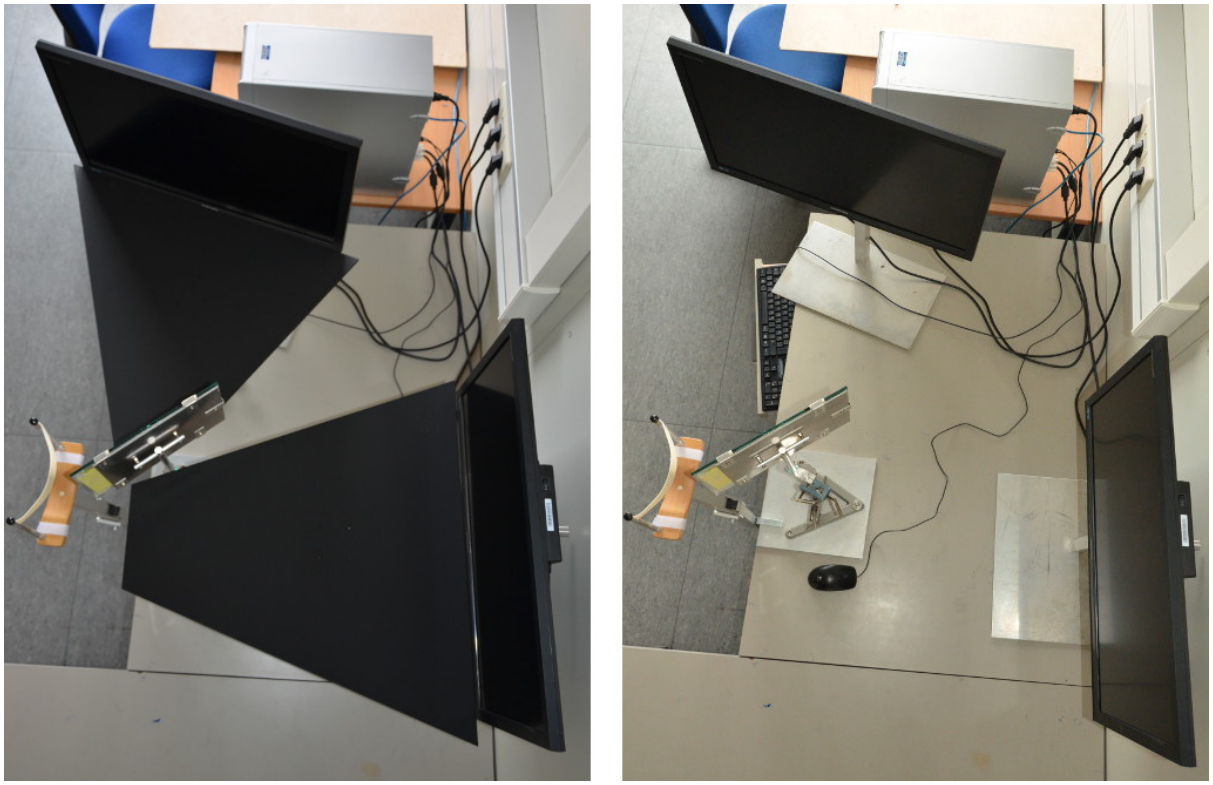

Figure 2.3.: View on the stereoscope from above. In the left image the bottoms of the viewing chamber bottoms are visible. The frontal viewing tunnel has a symmetrical trapeze shaped panel 18.7 cm at the observer's end, and 70 cm side length on the remaining edges. The left panel was an asymmetrical construction of 75 cm, 70 cm, 50 cm, and 20.6 cm with the following angles in the order of the listed lengths: $57°, 72°, 156°$, and $74°$. The right image shows the plain setup of the monitors and the mirror.

eye separation S and viewing angles α_1 and α_2 according to.

$$\begin{aligned}
\alpha_1 - \alpha_2 &= \frac{S}{D_1} - \frac{S}{D_2} \qquad (2.1)\\
&= \frac{S}{D_1} - \frac{S}{D_1 + \Delta D}\\
\frac{\alpha_1 - \alpha_2}{S} &= \frac{1}{D_1} - \frac{1}{D_1 + \Delta D}\\
&= \frac{D_1 + \Delta D - D_1}{D_1(D_1 + \Delta D)}\\
\frac{\Delta D \cdot S}{\alpha_1 - \alpha_2} &= D_1^2 + (\Delta D \cdot D_1)\\
D_1^2 &= \frac{\Delta D \cdot S}{\alpha_1 - \alpha_2} - (\Delta D \cdot D_1)\\
\Rightarrow D_1 &= \Delta D \pm \sqrt{\Delta D^2 + \frac{\Delta D \cdot S}{\alpha_1 - \alpha_2}} \qquad (2.2)
\end{aligned}$$

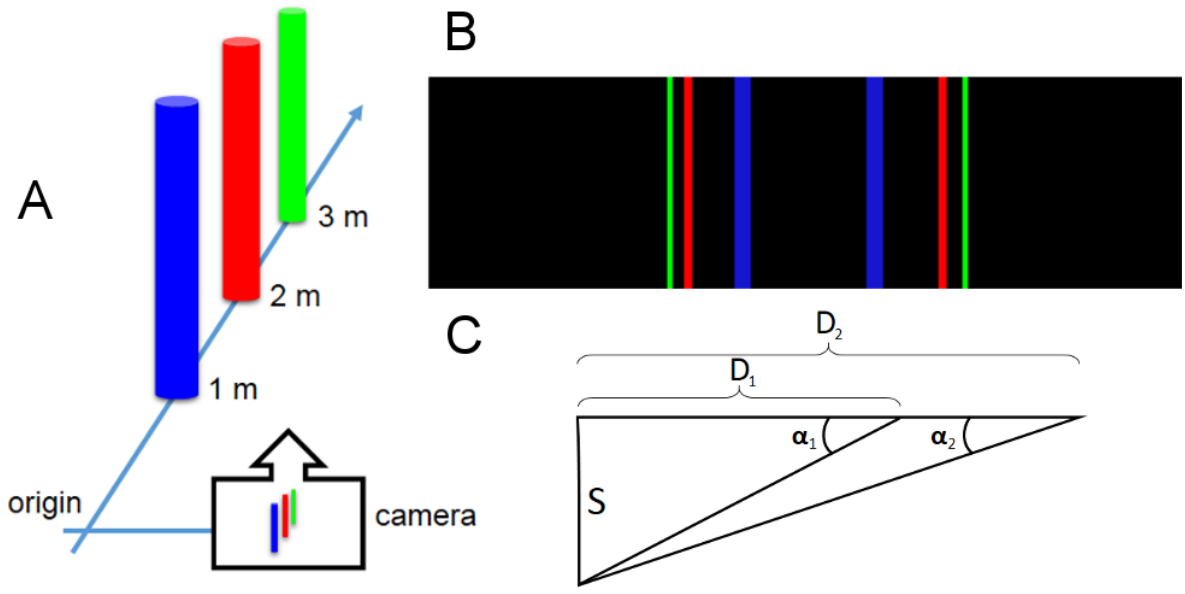

Figure 2.4.: **A**: A scene with three poles in distances 1, 2, and 3 meters. The test view was rendered after stepping aside by 0.3 m orthogonal to the line of the poles from the origin. **B**: Screenshot of the image displayed from both monitors. **C**: Schematic depiction of the triangular relation between the two eyes with an eye separation S and the two points in distance D_1 and D_2 to test for correctness of displayed disparity.

The calculation yielded a distance of 117.3 cm between the blue and the red pole, a distance of 120.86 cm between the red and the green pole and the distance of 228.6 cm between the blue and the green pole. Calculating the mean of these values yields 116.69 m with a variance of 2.31%. Given some disparities, the ratio of the corresponding objects could only be expected to reproduce the distance. From the measured disparities the calculated distance ratios were correct within the measurement errors. Therefore it could be concluded that the disparities were sufficiently well calculated by the software.

2.1.2. Stereoscope Software

The OpenSceneGraph library (Wang and Qian [2010]) which is largely based on the OpenGL library (Shreiner [2004]), was used to render the scenes. The software was develop in C++ using Visual Studio (Wiley Publishing [2008]). The focus of Hannig [2012] work was to develop a software to display any three-dimensional scene to the

screens and to run stereoscopic experiments. The two images of the stereogram must simulate a natural disparity depending on scene depth and the image seen through the mirror has to be inverted, mirrored along the vertical axis. Further, a library to render random dots has been developed to replace textures and to render surfaces into the screen space by using fixed sized and equally distributed dots.

2.1.2.1. Random-Dot-Limited-Lifetime Renderer

To use the software developed in HANNIG [2012] for the experiment, several changes to the code had to be made. So far, the Random-Dot-Limited-Lifetime Renderer was overriding in the function `DotExtractor::operator()` the OpenSceneGraph class `osg::Camera::DrawCallback` function to display dots with a randomized number within the interval between `_min_lifetime` and `_max_lifetime` dot lifetime. There, dot lifetimes were chosen short, below 100 ms, so an balance between newly created and dying dots could be reached after a few frames (given a frame rate of 60 Hz. In the present study, a fixed and long dot lifetime was supposed to be used. Using the original implementation, this would lead to a extinction of all dots at the same time and thus, the creation of a new generation of dots with the next frame. To account for this unwanted effect, at the beginning of a trial, the dot lifetimes now were randomized to value between zero and `_max_lifetime`. Therefore, variable `dead_dots` was introduced, counting the number of dying dots in each frame. At the beginning of a trial, when a new scene was loaded and the camera is directed towards the z-axis, the frustum (the rendered volume) changed completely and hence letting a large number of dots die. Now `dead_dots` could be compared with `_max_dots` (the number of maximally allowed dots) and the array `_dot_lifetime` that stores the lifetimes of all dots was reset. The whole rendering process was limited to a fixed frame rate of 60 Hz.

2.1.2.2. Experiment Implementation

Besides the Limited-Lifetime-Dot-Renderer, the software to conduct the experiment has been largely cleaned up and restructured. The following classes had been newly added to the software.

`Trial`: Objects of this class hold the data fields that are needed to execute each single trial. It contained the index of a trial, the tunnel shape, the acceleration in $^{m}/_{s^2}$ and in $^{m}/_{(\frac{1}{60}s)^2}$ (the acceleration related to the frame rate of 60 Hz), and the initial velocity in $^{m}/_{\frac{1}{60}s}$. It also stored the answer given during at the end of an trial.

`Experiment`: The class initiated the data fields of the actual acceleration and the according initial velocities. An array containing `Trial` objects was generated and ordered randomly. It also offered functions to safe the collected data during the experiment while ensuring not to overwrite already existing ones.

Now, the following classes built up the software to conduct experiments on the stereoscope.

`AgentManipulator`: The agent manipulator class allowed to explicitly control the camera position by move and turn functions instead of GUI events. The class `AgentManipulator` inherits from `osgGA::CameraManipulator` which contained the camera transformation matrix. Thus attaching the a `AgentManipulator` object to the scene tree allowed to position objects relative to the camera.

`BuildScene`: This class took care of loading scenes to the scene tree by attaching them to `osg::Switch` objects, which are able to switch between different scenes during running program execution. Further, it assured that the mouse cursor was hidden during an experiment and offered functions to display fog, light, and text tables and could be used to load supplementary images to the scene.

`Configuration`: To render the three-dimensional environment, the software had to be configured to match the setup in place. This class was implemented to set all necessary metrics from the stereoscopic setup to the renderer process (e.g., monitor distance, eye separation, etc.). Further, model file names and display mode were read and offered to the renderer and the experimental software.

`UserEventHandler`: This class overrode a number of functions of the `osgGA::GUIEventHandler` to catch events like keyboard and mouse input during software execution.

`Stereoskop:` This file contained the main executable function. In a brief summary, it first initialized an object of the class `Experiment`, `Configuration`, and `BuildScene`. Next, an `osg::Viewer` object was instantiated and an `AgentManipulator` object was attached to the camera in the scene tree. Further, the random dot renderer was initialized and the scenes were attached to the scene tree. Afterwards, the experiment loop starts.

2.1.2.3. Experiment Specific Addition

A blinding disc was used to obscure the end of the tunnel, here in a three-dimensionally rendered scene, the outer bounds of $zFar$, hence the farthest rendered dots. The disc was chosen to cover 20° visual angle and to be as distant inside of the tunnel as possible. In a three-dimensional setup, a close disc would obscure due to the disparity many dots to one eye that are visible to the other. Hence, the disc was set to a distance of about 6 m inside the tunnel, such that it does not intersect with the boundaries of the narrowing tunnel in the course of the trial. The distance of the disc was the same for all three tunnel shapes.

2.2. Experimental Design

In the setup described above was used in two series of experiments. In the following sections the experimental procedures together with used stimuli and the participants who took part in the sessions will be described.

2.2.1. Experimental Procedure

In general, the Festl et al. [2012] experimental design was replicated as far as possible. In the experiment of the cited study and the presented experiment, a method of Constant Stimuli was applied with a single stimulus procedure. Subjects watched dynamic random dot movies "flying" through a narrowing, straight or a widening corridor. Twelve different ego-acceleration levels were presented, ranging from -5.5 $^{m}/_{s^2}$ to 5.5 $^{m}/_{s^2}$ in 1 $^{m}/_{s^2}$ steps. One trial lasted three seconds and after each trial a text was displayed, asking the

participant to click left for deceleration and to click right for acceleration. After clicking there was a time lag of 200 ms before the next trial started.

The experiment per subject was held in four sessions to reduce fatigue. The overall experiment took about two and a half hours. Together, the first and the second session consisted of all in all 216 trials, six repetitions of all twelve accelerations, see section 2.2.2, in all three tunnels. While Festl et al. [2012] used the stair case algorithm best-PEST by Pentland [1980], in this work a more simplified algorithm was applied. After the first two sessions, a psychometric function was fitted, see section 2.3.1, and the detection threshold for each tunnel form was determined. These thresholds were transferred to the software at the beginning of the third session. Session three consisted of three repetitions of all twelve acceleration conditions of all 3 tunnels plus five repetitions of six accelerations conditions around the calculated threshold, in the range of presented acceleration conditions the three below and the three conditions about the threshold. This added up to 198 trials in session three. The same method was applied to session four. Thresholds were estimated, and in this case four repetitions of all threshold surrounding interval were used. This added up to 180 trials in session four. One experiment consisted of 594 trials, hence 198 trials per tunnel and in consequence 198 for data points for each fitting of the psychometric function. Every data point was evaluated from at least 18 measurements, and at most 27 measurements.

2.2.2. Stimuli

For generating the three-dimensional scenes, Blender (Blender Foundation), an open-source 3D computer graphics software was used. According to Festl et al. [2012], three different tunnel shapes were created, a straight tunnel, a widening and an expanding tunnel.

The straight tunnel had a diameter of 3.14 m along the entire length. The narrowing tunnel has a diameter of 4.14 m at the opening, narrowing down to a diameter of 3.14 m at a distance of 30.3 m. The widening tunnel has a diameter of 3.14 m at the opening, spreading to 4.14 m at a distance of 30.3 m. This resulted in an apical angle on 2° for

both the narrowing and the widening tunnel.

To ensure an equal distribution of dots throughout all three tunnel shapes, $zFar$ was set in the rendering configuration to 40.00 m. Further, to accommodate for the dots obscured to by the blinding disc, the surface was calculated that the disc occupies in the field of view. As the monitors were about 60 cm × 35 cm (2100 cm^2) and the disc about 20 cm in diameter (about 314 cm^2), the disc takes up about 15% of the screen. Therefore the dot density was setup to 1150 compared to 1000 dots in the experiment by Hannig [2012].

Twelve different levels of acceleration were used, ranging from -5.5 $^{m}/_{s^2}$ to $+5.5$ $^{m}/_{s^2}$ in steps of 1.0 $^{m}/_{s^2}$. To travel a distance of 30.3 m in 3 s, resulting in a mean velocity of $v_m = 10.1$ $^{m}/_{s}$ in each given acceleration condition, the initial velocity v_0 was calculated according to the following calculation. Given both

$$v(t) = v_0 + at \text{ and } s(t) = v_0 t + {}^1\!/_2\, at^2. \tag{2.3}$$

One can calculate

$$\begin{aligned} v_m &= \frac{s(t) - s(0)}{t} \\ &= \frac{v_0 t + {}^1\!/_2\, at^2}{t} \\ &= v_0 + {}^1\!/_2\, at \\ \Rightarrow v_0 &= v_m - {}^1\!/_2\, at. \end{aligned} \tag{2.4}$$

As the experiment was run at a monitor refresh rate of 60 frames per second, both initial velocities and accelerations had to be converted to a form of $^{m}/_{\frac{1}{60}s}$ and $^{m}/_{\frac{1}{60^2}s}$. Finally, a long dot lifetime was chosen to assure processing of optic flow.

2.2.3. Participants

The experiment was conducted with four participants, two female, two male, aged 22 to 29 years old. All participants had normal or corrected to normal vision. Participants

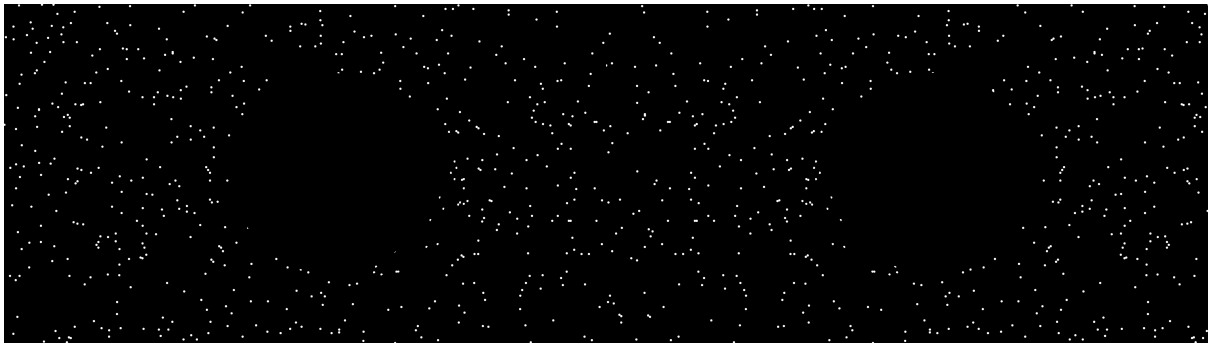

Figure 2.5.: Screenshot of the stimulus used in the experiment. The screenshot shows both images that were displayed to the left and the right monitor. When looking closely, on can see that the dot pattern was mirrored along a vertical line in the middle of the image (as the left image was viewed through the mirror). Further, the blinding disc was in the middle of each image. Dot size was increased for the screenshot (10 pixel), during the experiment dots size was set to 3 pixel.

AH, *FO* and *LP* were naive to the purpose of the study. Informed consent was obtained from each participant. Stereo vision was tested using random-dot stereograms taken from Julesz [1971].

2.2.4. Monocular Validating

In a second round of experiments, subjects *AH* and *TB* were tested on the same set of stimuli as in the first experiments. On the one hand, to rule out effects of the binocular viewing and the apparatus and on the other to compare the results to the work of Festl [2011], the experiment was repeated in a monocular setting. For the monocular testing, the dominant eye was determined by pointing binocularly to a distant object and stating the eye that points directly to the object.

2.3. Data Analysis

Data analysis was conducted using Matlab (MATLAB [2012]) and the Palamedes toolbox for for analyzing psychophysical data (Kingdom [2009]). After preprocessing the result data, psychometric functions were fitted. Next, standard error of the estimates and confidence intervals of the detection thresholds were calculated.

2.3.1. Fitting the Psychometric Function

Fitting the Psychometric Function creates a function that denotes performance on the task as a function of stimulus intensity x by $\psi(x)$. Using a sigmoidal function that describes the probability of correct stimulus detection $F(x)$ of stimulus x can be described. Defining the threshold α and the slope β of the fitted function, the performance underlying the sensory mechanism can be related as

$$\psi(x, \alpha, \beta) = F(x, \alpha, \beta). \tag{2.5}$$

Fitting a psychometric function can be done using a variety of sigmoidal functions. Here, the logistic function was deployed that is defined by

$$F_L(x, \alpha, \beta) = \frac{1}{1 + \exp(-\beta(x - \alpha))}. \tag{2.6}$$

Using the Maximum Likelihood criterion, psychometric functions were fitted to the collected data using the `PAL_PFML_Fit` routine. This routine used the iterative search algorithm Nelder-Mead Simplex Method to find the maximum in the likelihood function.

2.3.2. Standard Error of the Estimate

During the experiments, the stimulus range was adjusted to the participants performance. Hence, observed proportions correct at each of the stimulus intensities was directly used to generate bootstrap simulations of the experiment. The toolbox routine `PAL_PFML_BootstrapNonParametric` performs a non-parametric bootstrap method to determine standard errors on parameters of the fitted psychometric function. The standard error of the threshold with the threshold estimate $\hat{\alpha}_b$ resulting from bootstrap simulation b, the threshold that generated the sampling distribution α_g, and the number of simulations B is defined as

$$SE_{\hat{\alpha}} = \sqrt{\frac{\sum_{b=1}^{B}(\hat{\alpha}_b - \alpha_g)^2}{B}}. \tag{2.7}$$

The standard error of the slope of the fitted function was calculated the same way. Four hundred simulations were applied.

By assuming that the bootstrapped data were normally distributed, the bootstrapped data were used for two more evaluations. First, the confidence interval of the thresholds were determined by multiplying the standard error 1.96 as in

$$\text{Upper and lower 95\% Limit} \quad = \quad \bar{x} \pm (SE \cdot 1.96). \tag{2.8}$$

Further, the bootstrapped data were also used to determine if the mean of the thresholds were significantly different between the curves by using the student's t-test. t-test were only applied to compare neighboring curves.

3. Results

3.1. Participant's Reports

All participants commented that there were trials where it was extremely easy to come to a decision if accelerated or decelerated, while there were also trials where it seemed to display no acceleration at all. Subject *AH* described that in cases of strong acceleration or strong deceleration dots appeared as lines. *FO* stated that many of the trials are clear already at the very beginning. *FO* further reported that in some cases, the percept was contradictory at the beginning and end of a single trial. While *FO* would have voted for an acceleration at the beginning of a trial, at the end it appeared more to be a deceleration. *AH* said that deceleration seemed to be the prominent case of all trials, though stating the they surely must be equally distributed. Most participants made clear that they had some preference where to fixate, in the moments they chose one spot. For example both *LP* and *TB* preferred to fixate left of the central blinding disc.

All participant reported (without specific questioning) to have tried several strategies where to look during the trial. Overall, two strategies were described by all subjects. Either they fixated one single point during the whole trial, while it did not appear to be meaningful or in the possibility of the short trial time to choose several fixation point per trial. Changing the fixation area did not seem to lead to a different perception. Another strategy reported was to relax the eye looking rather in the middle of the screen and to come to a judgement from peripheral viewing. For *AH* it appeared to be harder to come to a decision when using peripheral viewing.

Subject *AH* interestingly reported that the black blind disc in the middle of the screen did not appear to be a flat surface but rather as a rolling ball. This subject had a

preference to look at the lower boarder of the blinding disc or in this case, of the rolling ball.

All participants commented that the overall experimental time passed quickly and easily and without any kind of noteworthy discomfort. Further, most subjects described some kind of a proprioceptic experience of the accelerations and decelerations.

3.2. Analysing the Collected Data

In this single stimulus procedure, the participants watched dynamic random dot display of a three seconds flight through a narrowing, a straight, and a widening tunnel. The experiment has been conducted in two different conditions, one in the binocular condition (stereoscopic), the other in the monocular condition.

In this section the results of the two series of experiments are presented and described. Psychometric functions have been fitted for each participant respectively, and for all participants together. Results of the three tunnel conditions (narrowing, straight, and narrowing) were compared and plotted together. In each plot presents three functions curves, the green curve shows the data of the narrowing tunnel, the red curves the straight tunnel and the blue curve the widening one. The vertical lines cross the threshold level of each curve respectively and serves only as a visual aid to better identify the value. The threshold level denotes the point of subjective equality (PSE). Horizontal lines describe the ±95% confidence interval (from center to center of the plus signs). The slope of the curves was generally neglect in further analysis.

3.2.1. Binocular Condition

In the first series of experiments, participants watched the stimuli binocularly. Four participants (AH, FO, LP, and TB) took part. The plots of the psychometric functions fitted are presented in figures 3.1, the psychometric function are presented for participant AH in figure 3.1A, for FO in 3.1B, for LP in 3.1C, and for subject TB in figure 3.1D. The number of measurements per acceleration condition is listed in table A.1 through

A.5.

From visual inspection it can be inferred that the fitting procedure described well the obtained data. Generally speaking, most of the data points are align to the fitted curves. Notably, in the curves for the straight tunnel, all participants showed some amount of wrong judgment of the ego-acceleration condition of 4.5 $^{m}/_{s^2}$. The blue curve (widening tunnel) in figure 3.1A for participant *AH* does not reach a 100% level for answer "acceleration" for the highest ego-acceleration 5.5 $^{m}/_{s^2}$, yielding a low slope at the level of the threshold. In figure 3.1C and 3.1D, the red curve stays above the green curve until a level -2.5 $^{m}/_{s^2}$ and -1.5 $^{m}/_{s^2}$ respectively.

Further, confidence intervals generally did not overlap. Only in the case of the green and the red curve in figure 3.1C, confidence intervals overlap marginally. A student's t-test still yielded a significantly different with a $p < 0.01$. Hence, it can be stated that the curves are well separated for all tunnel conditions and the means of the curves are all significantly different by applying the student's t-test with $p < 0.01$.

All participants yielded a point of subjective equality for the straight tunnel between -0.5 and 0.0 $^{m}/_{s^2}$. For the narrowing tunnel, the PSE was around -1.0 $^{m}/_{s^2}$. And for the widening tunnel, the PSE was more spread, yielding values between 0.8779 $^{m}/_{s^2}$ for subject *FO* and 2.1320 $^{m}/_{s^2}$ for subject *AH* in its extremes.

Figure 3.2 plots of the fitted psychometric functions for all subjects data together. Here, visual inspection shows a clear separation of the curves. Most of the data points are well aligned with the fitted curves. As already described above, in the ego-acceleration condition 4.5 $^{m}/_{s^2}$ in the straight tunnel (red curve), the data point shows a strong deviation from the fitted curve. The confidence interval 95% of all curves were smaller than in the individual plots and were well separated between the curves. Also t-testing the differences yielded that the thresholds of all curves are significantly different with $p < 0.01$. The PSE of the narrowing tunnel was -1.0841 $^{m}/_{s^2}$, for the straight tunnel -0.3074 $^{m}/_{s^2}$, and for the widening tunnel 1.5612 $^{m}/_{s^2}$. An overview of the thresholds for each participant including the overall evaluation for each tunnel condition is given in table 3.1.

Participant	Tunnel		
	Narrowing	Straight	Widening
AH	-1.1142	-0.0776	2.1320
FO	-1.1495	-0.4387	0.8779
LP	-0.9257	-0.2668	1.6639
TB	-1.1490	-0.4568	1.5958
All	**-1.0841**	**-0.3074**	**1.5612**

Table 3.1.: Thresholds determined in the experiments in the binocular condition for the three tunnel conditions for all participants and the data of all participants together.

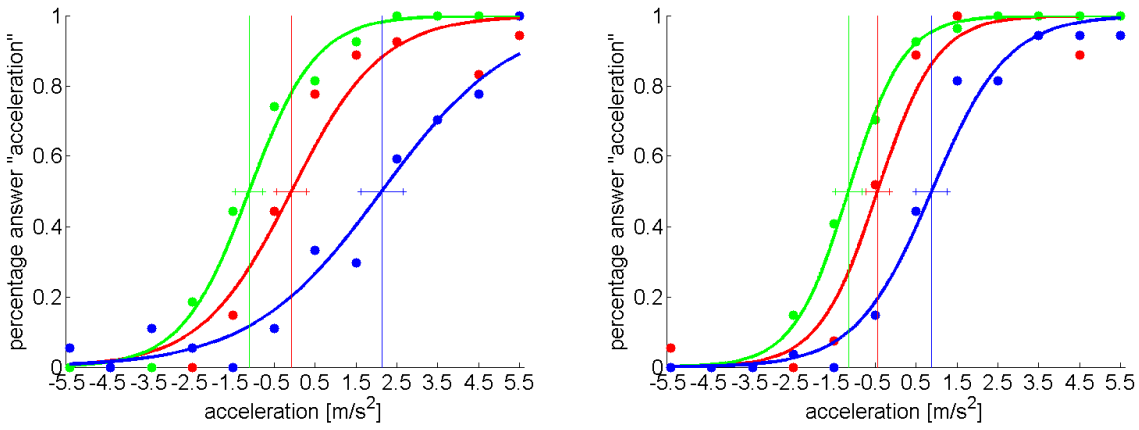

(a) AH (b) FO

(c) LP (d) TB

Figure 3.1.: Psychometric functions fitted to the data of the experiment in the binocular condition for subjects *AH*, *FO*, *LP*, and *TB*. The x-axis denotes the ego-acceleration conditions, the y-axis denotes the percentage of the answer "Acceleration". *Green*: narrowing, *Red*: straight, *Blue*: widening.

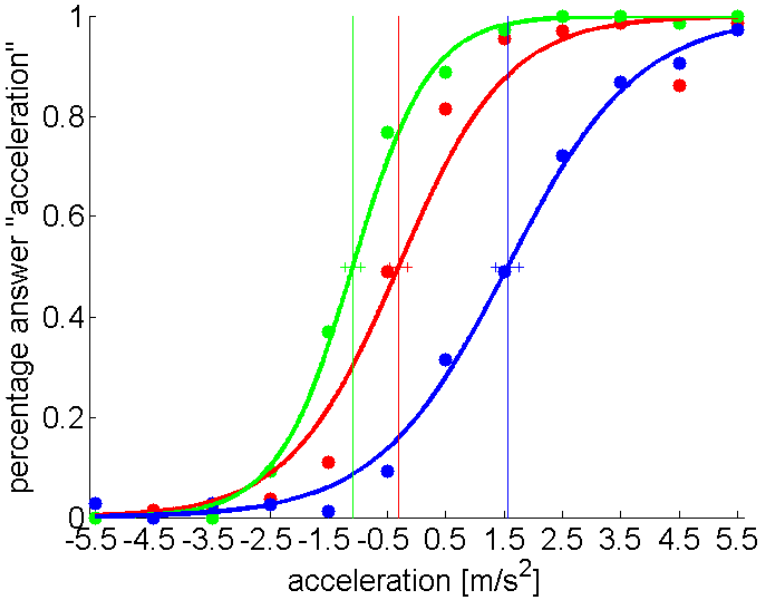

Figure 3.2.: Psychometric functions fitted to all the data collected in the experiment in the binocular condition. The x-axis denotes the ego-acceleration conditions, the y-axis denotes the percentage of the answer "Acceleration". *Green*: narrowing, *Red*: straight, *Blue*: widening.

3.2.2. Monocular Condition

In the second series of experiments, participants watched the stimuli monocularly. Two participants (AH and TB) took part. The plots of the corresponding psychometric functions fitted are presented in figures 3.3, the psychometric function are presented for participant AH in figure 3.3A and for subject TB in figure 3.3B. The plotted functions have the same structure as in section 3.2.1. The number of measurements per acceleration condition is listed in table A.6 through A.8.

From visual inspection it can be inferred also in the monocular condition that the fitting procedure described well the obtained data. Generally speaking, most of the data points are align to the fitted curves, with the exception of the the red curve in figure 3.3 and the green curve in figure 3.3B. Just as in the binocular condition, both participants showed some amount of wrong judgments in the ego-acceleration condition of 4.5 $^{m}/_{s^2}$ in the curves for the straight tunnel. The blue curve (widening tunnel) in figure 3.3B for participant TB does not reach a 100% level for answer "acceleration" for the highest

Participant	Tunnel		
	Narrowing	Straight	Widening
AH	-1.1125	-0.6265	2.1925
TB	-0.4665	0.2168	2.2751
All	**-0.7927**	**-0.2100**	**2.2342**

Table 3.2.: Thresholds determined in the experiments in the monocular condition for the three tunnel conditions for all participants and the data of all participants together.

ego-acceleration 5.5 $^{m}/_{s^2}$. In figure 3.3A, the red curve stays above the green curve until a level of -1.5 $^{m}/_{s^2}$.

In the case of the green and the red curve in figure 3.3A, confidence intervals overlap. A student's t-test still yielded a significantly different with a $p < 0.01$. Despite this case, all curves are well separated for all tunnel conditions and the means of the curves are all significantly difference by applying the student's t-test with $p < 0.01$.

Except for the widening tunnel, the PSE of both subjects deviated strongly for the narrowing and the widening tunnel, see table 3.2.

Figure 3.4 plots of the fitted psychometric functions for all collected data together. Here, visual inspection shows a clear separation of the curves. The fitting of the psychometric function matches the data points better than in the individual plots. As in the binocular condition,the ego-acceleration condition 4.5 $^{m}/_{s^2}$ in the straight tunnel (red curve) shows a strong deviation between the fitted curve and the data point. The confidence intervals 95% of all curves were small and did not overlap. Also t-testing the differences yielded that the thresholds of all curves were significantly different with $p < 0.01$. The PSE of the narrowing tunnel was -0.7927 $^{m}/_{s^2}$, for the straight tunnel -0.2100 $^{m}/_{s^2}$, and for the widening tunnel 2.2342 $^{m}/_{s^2}$.

An overview of all thresholds for each participant including the overall evaluation for each tunnel condition is given in table 3.2.

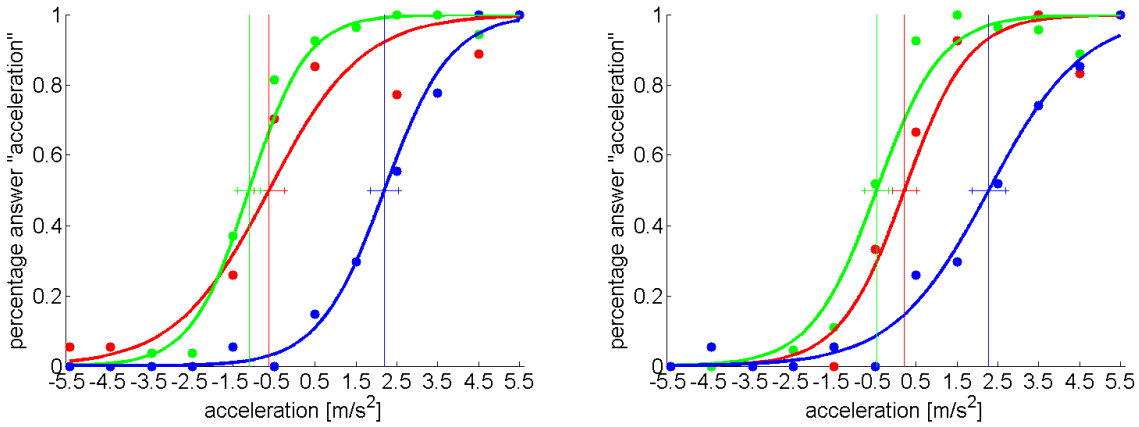

(a) AH mono (b) TB mono

Figure 3.3.: Psychometric functions fitted to the data of the experiment in the monocular condition for subjects AH and TB. The x-axis denotes the ego-acceleration conditions, the y-axis denotes the percentage of the answer "Acceleration". *Green*: narrowing, *Red*: straight, *Blue*: widening. psychometric functions fitted to the data of experiment 2 for subjects AH and TB.

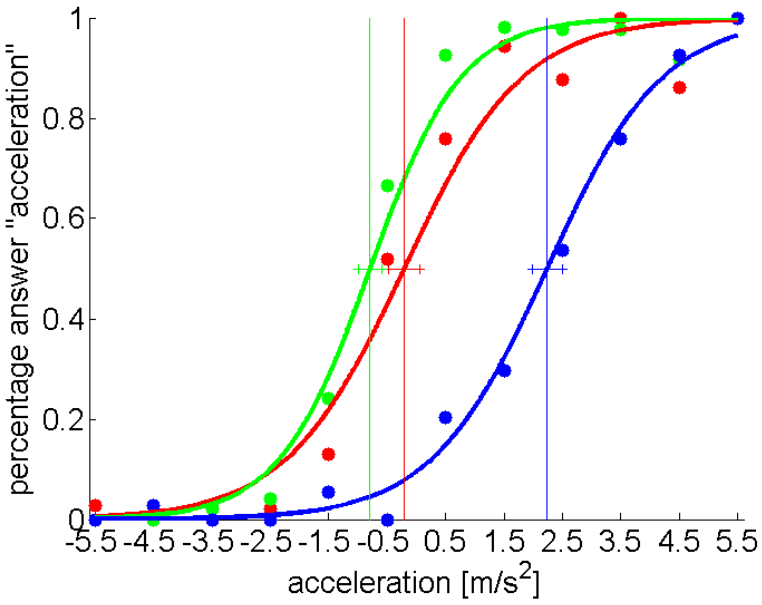

Figure 3.4.: Psychometric functions fitted to all the data collected in the experiment in the monocular condition. The x-axis denotes the ego-acceleration conditions, the y-axis denotes the percentage of the answer "Acceleration". *Green*: narrowing, *Red*: straight, *Blue*: widening.

4. Discussion

In the following section the results of the main experiment in the binocular viewing condition will be discussed. These results will be compared to the findings to the recent study by Festl et al. [2012]. Further, the results of the second series of experiments will be discussed. Finally, the implications to the integration of the two cues, optic flow and binocular disparity, present in the stimuli will be outlined.

4.1. Experiment in the Binocular Condition

The data collected in the experiments with binocular vision showed that the perceived ego-acceleration depended on the three-dimensional structure of the tunnels presented in the stimuli.

Looking at the data presented in figure 3.2, the detection threshold of the fitted psychometric function of the data for the straight tunnel matched, as expected, an acceleration of 0 $^{m}/_{s^2}$, with some deviation to a negative acceleration. Hence, in the straight tunnel, a negative acceleration was perceived as a deceleration and a positive acceleration as an actual ego-acceleration.

However, thresholds for the narrowing tunnel were shifted away from zero acceleration (-1.0841 $^{m}/_{s^2}$). Hence, an deceleration up to approximately -1 $^{m}/_{s^2}$ was perceived as an acceleration to a percentage above chance level. When flying through the narrowing tunnel, the distance of the observer to the tunnel walls decreased over time and consequently, the optic flow was increased.

In the case of the widening tunnel the result was inverted. Thresholds were shifted towards an acceleration value of 1.5612 $^{m}/_{s^2}$. An positive acceleration up to a level of

approximately 1.5 $^{m}/_{s^2}$ was recognized as deceleration. While flying along the widening tunnel, tunnel walls diverged from the observer with the effect that optic flow was reduced during over the time of a trial.

Finally, the detection thresholds of the fitted psychometric functions from the data of the narrowing and the widening tunnel showed an asymmetrical shift in relation to the threshold of the straight tunnel. The threshold of the widening tunnel was shifted about 0.5 $^{m}/_{s^2}$ further towards an acceleration than the threshold of the narrowing tunnel. It was shifted towards a deceleration.

4.2. Comparison to Previous Findings

When comparing the actual results to the finding in the work by Festl et al. [2012] (see figure 4.1), several implications could be drawn.

In both the present study as well as in the study by Festl et al. [2012], thresholds for the conic tunnels were shifted away from the zero acceleration. This shift suggested a confusion of ego-acceleration and three-dimensional structure of the tunnel. However, under stereoscopic viewing this confusion was strongly reduced. In the cited study, thresholds for the narrowing tunnel were around -2.5 $^{m}/_{s^2}$, for the widening tunnel at around 3.3 $^{m}/_{s^2}$. Hence for both tunnels we could report a reduction of about 1.5 $^{m}/_{s^2}$. In the Festl et al. [2012] study, results were in fair quantitative agreement with the shifts predicted from the matched-filter approach. Assuming that theoretical predictions would have yielded similar results when calculating thresholds according to equation 1.2 for the stimuli in the present study, the results could not be explained from the matched-filter approach for estimation of ego-acceleration. Furthermore, although depth information was present in the stimuli from binocular disparity, acceleration rate seemed to be neglected at least to some degree.

A small asymmetry of the shifts of the thresholds for the conic tunnels could be reported already in the Festl et al. [2012] work. This asymmetry was largely amplified in the findings of the present study as discussed above. One possible explanation for this asymmetry could be found in the geometry of the used stimuli. Both narrowing

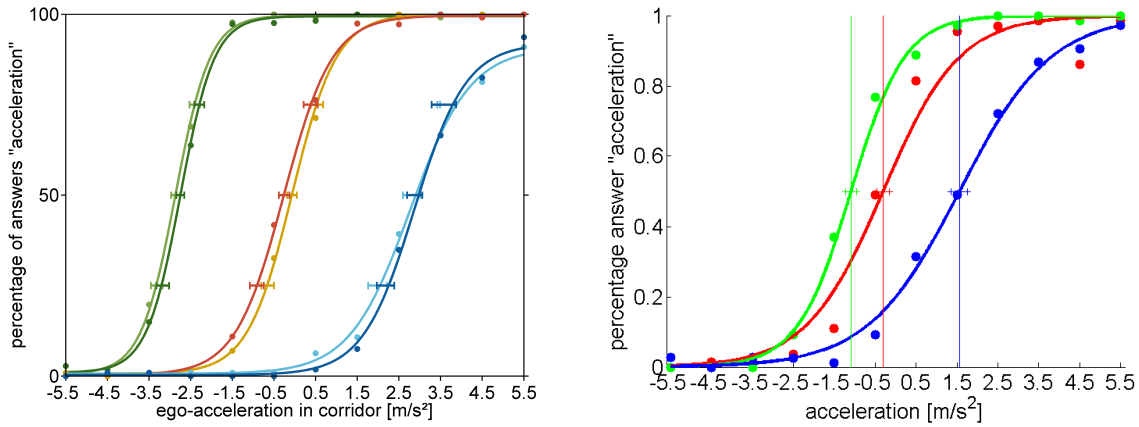

(a) Psychometric functions of the FESTL ET AL. [2012] study.

(b) Psychometric functions of the present study.

Figure 4.1.: Comparison of the results of the recent study by FESTL ET AL. [2012] and the result of the present study. *Left*: Fitted psychometric functions for all three subjects together, from Experiment 2 (monocular viewing) in FESTL ET AL. [2012]. *Green*: narrowing tunnel, *red*, *yellow*: straight tunnel, *blue*: widening tunnel; dark colors: long dot lifetime, light colors: short dot lifetime. Horizontal "error bars" show 99% confidence intervals at the response levels 0.25, 0.5, and 0.75. *Right*: Psychometric functions fitted to all the data collected in the experiment in the binocular condition. The x-axis denotes the ego-acceleration conditions, the y-axis denotes the percentage of the answer "Acceleration". *Green*: narrowing, *Red*: straight, *Blue*: widening.

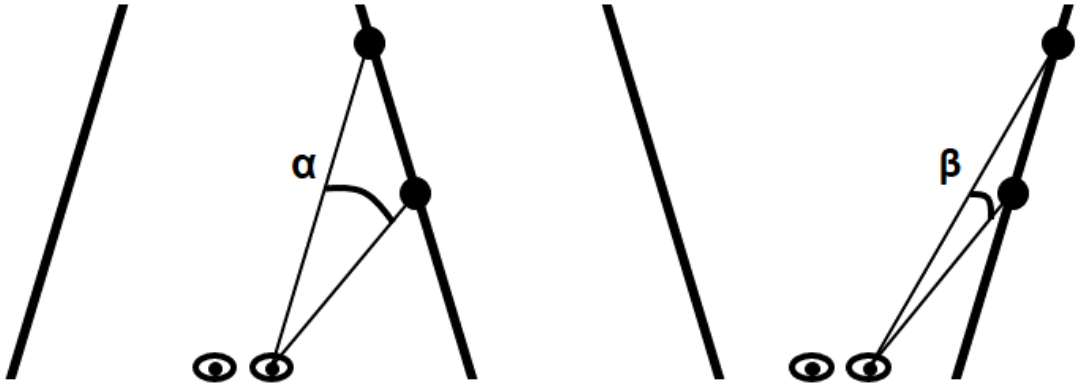

(a) Narrowing Tunnel (b) Widening Tunnel

Figure 4.2.: Comparison of visual angles between two neighboring points along the tunnel walls. In a narrowing tunnel, a visual angle α is bigger compared to a visual angle β of two neighboring points in the same distance in a widening tunnel.

and widening tunnel had an apical angle of 2°. When considering two neighboring points along the tunnel wall, the visual angle between the two points was larger in the narrowing tunnel. However, this angle was smaller for the widening tunnel, see figure 4.2. This difference might have resulted in a lowered accuracy of depth estimation. This conception seemed apparent from consideration about geometry. The same apical angles of the two tunnel shapes might not have an equivalent effect on depth perception.

4.3. Experiment in the Monocular Condition

The second series of experiments using monocular viewing was conducted for two purposes. Firstly, to replicate the results of Festl et al. [2012] and secondly, to rule out effects of the new stereoscopic setup compared to the setup used in the previous work as they are presented in the above section. However, the data did not support these hypotheses.

The data collected from two subjects showed a similar trend in the fitted psychometric functions as in the binocular viewing condition. The threshold for the straight tunnel was even closer to zero compared to the result in the main experiment. The shift of

the threshold for the narrowing tunnel was even further reduced, while the shift of the widening tunnel was further increased. Hence, the asymmetry was even stronger than in the binocular viewing condition. This finding could also be explained as above where depth information could be reduced in the widening tunnel.

Additionally, The two subjects both took part yet in the first series of experiments. Accordingly, they watched already the stimuli in stereo vision and it could be assumed that they had some knowledge about the three-dimensional structure of the presented stimuli. This prior knowledge could have lead to a better understanding of the three-dimensional structure of the stimuli as originally formulated by von Hornbostel [1927].

A prominent difference between the experimental setup of the Festl et al. [2012] study and the present study should be noted. The field of view in the old setup subtended a visual angle of 23°, both in horizontal and vertical direction. In the present study, the stimuli subtended approximately 41° horizontal visual angle and 24° vertical visual angle. This resulted in nearly a doubling of the visual angle in the horizontal direction. As Koenderink and van Doorn [1987] reported, the field of view must be considered as a factor in the estimation of depth and ego-motion. Further, the human visual field is elliptical along the horizontal axis, hence the extended horizontal field could be assumed of to play some role.

4.4. Implications for Cue Integration

Cue integration of optic flow and stereopsis appeared to support the discrimination of acceleration and three-dimensional geometry. An accumulation of information by probability summation could result from binocular vision, the two eyes collect more information about the world than only one in monocular viewing. Time-to-collision estimates from observing single dots could also be accumulated with depth information from binocular disparity. In a cooperative approach of cue integration, it could be stated that time-to-collision estimates were improved when watching single dots binocularly. Finally, the Bayesian model offers a statistical approach to explain the reduction and yet not full compensation of the found effect. It gives further hints for explaining the effect observed

in the monocular viewing condition that did not replicate recent findings and was very similar to the results from the binocular viewing condition.

5. Conclusion

In conclusion, this study was conducted to investigate if subjects used information from binocular disparity and optic flow to judge ego-acceleration. For this purpose, a stereoscopic setup was modified and validated for accuracy of disparities. Psychometric functions of the perception of ego-acceleration in a straight, a narrowing, and a widening tunnel were fitted. The results of the present study showed that subjects confused effects from ego-acceleration and three-dimensional scene geometry in conic tunnels.

To a large extend the experimental design was similar to the recent study by Festl et al. [2012]. This study demonstrated that performance could be predicted by the matched-filter approach for the estimation of ego-acceleration that neglected depth information. In the present study, the thresholds of the psychometric functions of the narrowing tunnel were shifted towards a deceleration and the thresholds of the widening tunnel were shifted towards a acceleration. Nevertheless, the thresholds of both conic tunnels approached the one of the straight tunnel. Hence, the matched-filter approach could not describe the results. A full compensation of the shifts by the acceleration rate approach for the estimation of ego-acceleration could not be observed.

However, some integration of the offered cues, binocular disparity and optic flow, must have occured. The present study was not designed to investigate in how far this cue integration occured or how it could be explained. Still, some cooperation of the cue or some information accumulation of the cues must have taken place. Also, a Bayesian integration of cues could be postulated.

Further, it was shown that the three-dimensional geometry of the tunnels played a role in the performance of the subjects. An asymetry was found between the narrowing and the widening tunnel although they were thought to generate similar results. From the

results, it could be concluded, that the apical of the widening should have been chosen smaller to achieve symmetrical shifts of the detection thresholds of the conic tunnels.

To finalize this work, a few future aspects should be noted. Two studies will be conducted as a direct follow up the here presented work. First, an experiment will be conducted in which the random-dot tunnels will be replaced by a street scene with buildings. The objects along the street will be scaled smaller or larger with the travelled distance. In this simulated natural environment setup, object recognition and scene segmentation are expected to help reduce further the confusion of ego-acceleration and scene geometry. In a second experiment, subjects will be accelerated in corrugated tunnels while they are instructed to compensate the perceived acceleration with a joystick. The corrugated tunnels are thought to offer better depth perception and the option to actively control the motion might also play a role in the estimation of ego-acceleration.

Lastly, the extend of cue integration regarding optic flow and stereo vision should be investigated. There are some signs that additional cues like continous textures, objects, and prior knowledge about the world would further support cue integration. Also the underlying mechanism are an important field for further studies including considerations about the neural correlates of this integration. The found asymetry needs to be further investigated. And finally, a computational algorithm needs to be developed to predict the perception of ego-acceleration from the integration of optic flow and stereo cues.

A. Number of Measurements

A.1. Number of Measurements in Binocular Viewing

Tunnel	Acceleration in $^m/_{s^2}$											
	-5.5	-4.5	-3.5	-2.5	-1.5	-0.5	0.5	1.5	2.5	3.5	4.5	5.5
Narrowing	18	18	27	27	27	27	27	27	18	18	18	18
Straight	18	18	18	27	27	27	27	27	27	18	18	18
Widening	18	18	18	18	18	27	27	27	27	27	27	18

Figure A.1.: Number of Measurements of subject *AH* in the binocular viewing condition.

Tunnel	Acceleration in $^m/_{s^2}$											
	-5.5	-4.5	-3.5	-2.5	-1.5	-0.5	0.5	1.5	2.5	3.5	4.5	5.5
Narrowing	18	18	27	27	27	27	27	27	18	18	18	18
Straight	18	18	27	27	27	27	27	27	18	18	18	18
Widening	18	18	18	27	27	27	27	27	27	18	18	18

Figure A.2.: Number of Measurements of subject *FO* in the binocular viewing condition.

Tunnel	Acceleration in $^m/_{s^2}$											
	-5.5	-4.5	-3.5	-2.5	-1.5	-0.5	0.5	1.5	2.5	3.5	4.5	5.5
Narrowing	18	18	27	27	27	27	27	27	18	18	18	18
Straight	18	18	18	27	27	27	27	27	27	18	18	18
Widening	18	18	18	18	18	27	27	27	27	27	27	18

Figure A.3.: Number of Measurements of subject *LP* in the binocular viewing condition.

Tunnel	Acceleration in $^m/_{s^2}$											
	-5.5	-4.5	-3.5	-2.5	-1.5	-0.5	0.5	1.5	2.5	3.5	4.5	5.5
Narrowing	18	18	27	27	27	27	27	27	18	18	18	18
Straight	18	18	18	27	27	27	27	27	27	18	18	18
Widening	18	18	18	18	22	27	27	27	27	27	23	18

Figure A.4.: Number of Measurements of subject TB in the binocular viewing condition.

Tunnel	Acceleration in $^m/_{s^2}$											
	-5.5	-4.5	-3.5	-2.5	-1.5	-0.5	0.5	1.5	2.5	3.5	4.5	5.5
Narrowing	72	72	108	108	108	108	108	108	72	72	72	72
Straight	72	72	81	108	108	108	108	108	99	72	72	72
Widening	72	72	72	81	85	108	108	108	108	99	95	72

Figure A.5.: Number of Measurements summed over subjects AH, FO, LP, and TB in the binocular viewing condition.

A.2. Number of Measurements in Binocular Viewing

Tunnel	Acceleration in $^m/_{s^2}$											
	-5.5	-4.5	-3.5	-2.5	-1.5	-0.5	0.5	1.5	2.5	3.5	4.5	5.5
Narrowing	18	18	27	27	27	27	27	27	18	18	18	18
Straight	18	18	27	27	27	27	27	27	18	18	18	18
Widening	18	18	18	18	18	27	27	27	27	27	27	18

Figure A.6.: Number of Measurements of subject AH in the monocular viewing condition.

Tunnel	Acceleration in $^m/_{s^2}$											
	-5.5	-4.5	-3.5	-2.5	-1.5	-0.5	0.5	1.5	2.5	3.5	4.5	5.5
Narrowing	18	18	18	22	27	27	27	27	27	23	18	18
Straight	18	18	18	22	27	27	27	27	27	23	18	18
Widening	18	18	18	18	18	22	27	27	27	27	27	23

Figure A.7.: Number of Measurements of subject TB in the monocular viewing condition.

Tunnel	Acceleration in $^m/_{s^2}$											
	-5.5	-4.5	-3.5	-2.5	-1.5	-0.5	0.5	1.5	2.5	3.5	4.5	5.5
Narrowing	36	36	45	49	54	54	54	54	45	41	36	36
Straight	36	36	45	49	54	54	54	54	45	41	36	36
Widening	36	36	36	36	36	49	54	54	54	54	54	41

Figure A.8.: Number of Measurements summed over subjects AH and TB in the monocular viewing condition.

Bibliography

The websites referred to below were last accessed on March 27, 2013. In case of unavailability at a later time, we recommend visiting the Internet Archive.

Blender Foundation. *Blender v2.49a*. URL `http://www.blender.org`.

Heinrich H Bulthoff and Hanspeter A Mallot. Integration of depth modules: stereo and shading. *JOSA A*, 5(10):17491758, 1988.

Aurore Capelli, Alain Berthoz, and Manuel Vidal. Estimating the time-to-passage of visual self-motion: Is the second order motion information processed? *Vision Res.*, 50 (9):91423, April 2010. doi: 10.1016/j.visres.2010.02.011.

Freya Festl. Erkennung der Eigenbeschleunigung durch optischen Fluss, 2011.

Freya Festl, Fabian Recktenwald, Chunrong Yuan, and Hanspeter A Mallot. Detection of linear ego-acceleration from optic flow. *J Vis*, 12(7), 2012. doi: 10.1167/12.7.10.

Matthias O. Franz, Javaan S. Chahl, and Holger G. Krapp. Insect-Inspired Estimation of Egomotion. *Neural Computation*, 16(11):22452260, 2004.

Matthias D. Hannig. Entwicklung und Validierung eines spiegelstereoskopischen Virtual-Reality Aufbaus, 2012.

B. Julesz. *Foundations of Cyclopean Perception: [With 3-D Glasses]*. Mit Press, 1971. ISBN 0-226-41527-9.

M K Kaiser and H Hecht. Time-to-passage judgments in nonconstant optical flow fields. *Percept Psychophys*, 57(6):81725, August 1995.

Frederick A. A. Kingdom. *Psychophysics: A Practical Introduction*. Academic Press, first edition, 2009. URL `http://www.palamedestoolbox.org`.

J J Koenderink and A J van Doorn. Facts on optic flow. *Biol Cybern*, 56(4):24754, 1987.

Joel Kollin and Ari Hollander. Re-engineering the Wheatstone stereoscope. volume 6490, page 9, February 2007.

MATLAB. *version 8.00.783 (R2012b)*. The MathWorks Inc., Natick, Massachusetts, 2012.

A Pentland. Maximum likelihood estimation: the best PEST. *Percept Psychophys*, 28 (4):3779, October 1980.

B J Rogers and T S Collett. The appearance of surfaces specified by motion parallax and binocular disparity. *Q J Exp Psychol A*, 41(4):697717, November 1989.

Dave Shreiner. *OpenGL reference manual: the official reference document to OpenGL, version 1.4*. Addison-Wesley, 4 edition, 2004. ISBN 9780321173836.

J S Tittle and M L Braunstein. Recovery of 3-D shape from binocular disparity and structure from motion. *Percept Psychophys*, 54(2):15769, August 1993.

Erich M von Hornbostel. The unity of the senses. *Psyche*, 7(4), 1927.

R. Wang and X. Qian. *OpenSceneGraph 3.0: Beginner's Guide*. December 2010. ISBN 978-1-849512-82-4.

W H Warren, M W Morris, and M Kalish. Perception of translational heading from optical flow. *J Exp Psychol Hum Percept Perform*, 14(4):64660, November 1988.

Charles Wheatstone. The Bakerian Lecture - Contributions to the Physiology of Vision.Part the Second. On Some Remarkable, and Hitherto Unobserved, Phenomena of Binocular Vision (Continued). *Philosophical Transactions of the Royal Society of London*, 142:117, 1852.

Wiley Publishing. Visual Studio ®2008. *Framework*, page 1032, 2008.

Chen Ping Yu, William K Page, Roger Gaborski, and Charles J Duffy. Receptive field dynamics underlying MST neuronal optic flow selectivity. *J. Neurophysiol.*, 103(5): 2794807, May 2010. doi: 10.1152/jn.01085.2009.

List of Figures